Ecological Applications, 18(6), 2008, pp. 1420–1435

THE STRUCTURE OF TURBULENCE NEAR A TALL FOREST EDGE: THE BACKWARD-FACING STEP FLOW ANALOGY REVISITED

Matteo Detto,[1] Gabriel G. Katul,[2,3,5] Mario Siqueira,[2,4] Jehn-Yih Juang,[2] and Paul Stoy[2]

[1]*Dipartimento di Ingegneria Idraulica, Ambientale e del Rilevamento, Politecnico di Milano, Italy*
[2]*Nicholas School of the Environment and Earth Sciences, Box 90328, Duke University, Durham, North Carolina 27708 USA*
[3]*Department of Civil and Environmental Engineering, Pratt School of Engineering, Duke University, Durham, North Carolina 27708 USA*
[4]*Departamento de Engenharia Mecânica, Universidade de Brasília, Brazil*

Abstract. Flow disturbances near tall forest edges are receiving significant attention in diverse disciplines including ecology, forest management, meteorology, and fluid mechanics. Current theories suggest that near a forest edge, when the flow originates from a forest into a large clearing, the flow retains its forest canopy turbulence structure at the exit point. Here, we propose that this framework is not sufficiently general for dense forested edges and suggest that the flow shares several attributes with backward-facing step (BFS) flow. Similar analogies, such as rotor-like circulations, have been proposed by a number of investigators, though the consequences of such circulations on the primary terms in the mean momentum balance at the forest clearing edge have rarely been studied in the field. Using an array of three triaxial sonic anemometers positioned to measure horizontal and vertical gradients of the velocity statistics near a forest edge, we show that the flow structure is more consistent with an intermittent recirculation pattern, rather than a continuous rotor, whose genesis resembles the BFS flow. We also show that the lateral velocity variance, $\overline{v'^2}$, is the moment that adjusts most slowly with downwind distance as the flow exits from the forest into the clearing. Surprisingly, the longitudinal and vertical velocity variances ($\overline{u'^2}$ and $\overline{w'^2}$) at the forest edge were comparable in magnitude to their respective values at the center of a large grass-covered forest clearing, suggesting rapid adjustment at the edge. Discussions on how the forest edge modifies the spectra and co-spectra of momentum fluxes, effective mixing length, and static pressure are also presented.

Key words: backward-facing step flow analogy; forest edges; mean momentum transfer; recirculation zone.

Introduction

Studies of turbulent transport processes at the biosphere–atmosphere interface are becoming increasingly ecological in scope, whether be it for measuring the flux of carbon and water (Baldocchi et al. 2001) or for determining long-distance seed and pollen dispersal by wind (Nathan et al. 2002, 2005, Soons et al. 2004, Nathan and Katul 2005, Williams et al. 2006). While the statistical properties of turbulence in the atmospheric surface layer (ASL) have been extensively studied over homogeneous surfaces, disturbances to the flow created by transitions from one surface cover to another remains a subject of theoretical and experimental research (Garratt 1990, 1994, Gardiner 1994, Judd et al. 1996, Veen et al. 1996, Dwyer et al. 1997, Patton et al. 1998, Lee 2000, Belcher et al. 2003, Coceal and Belcher 2005). One such flow disturbance are tall forest edges—now gaining significant attention in many research areas within ecology, hydrology, meteorology, and fluid mechanics because of their relevance to not only problems such as seed and pollen dispersal in gaps (Nathan et al. 2005, Williams et al. 2006), but also forest fragmentation effects on abiotic and biotic processes (Malcom 1998), forest felling management (Flesch and Wilson 1999), enhanced dry deposition of atmospheric pollutants (De Ridder et al. 2004), and up-scaling turbulent fluxes and mean meteorological states from patchy land surfaces in boundary layer models (Klaassen 1992, Garratt 1994, Klaassen and Claussen 1995), to name few applications.

Motivated by such applications, field and laboratory experiments have already been conducted in the past three decades to analyze the bulk flow properties near step changes in surface roughness. These early studies primarily focused on the growth of the so-called "internal boundary layer" or IBL (Garratt 1990), a region influenced by the abrupt roughness and concomitant surface shear stress jump. Roughness tran-

Manuscript received 6 June 2006; revised 24 January 2007; accepted 26 January 2007. Corresponding Editor: H. P. Schmid. For reprints of this Invited Feature, see footnote 1, p. 1338.
[5] E-mail: gaby@duke.edu

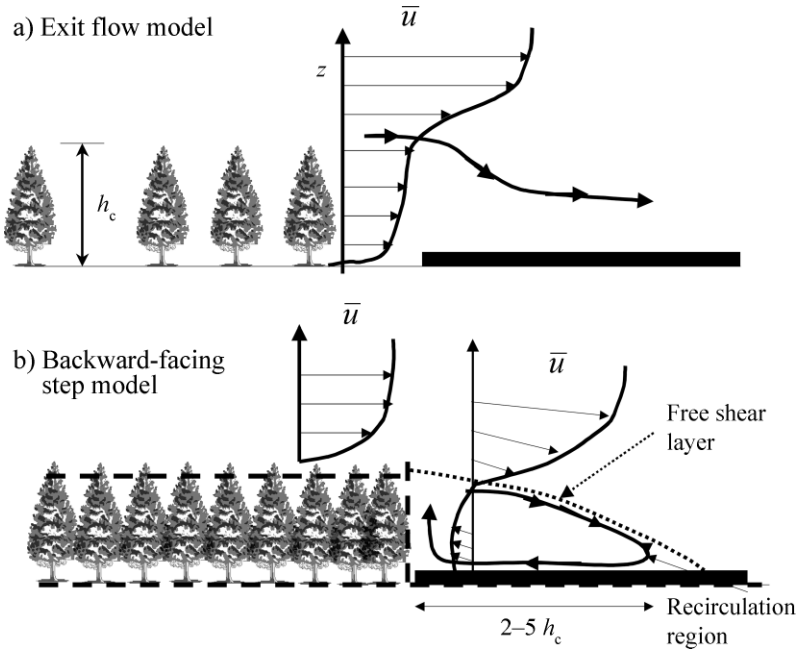

FIG. 1. Two conceptual models for the structure of turbulence near forest edges. (a) The exit flow model in which the mean flow near the edge retains its canopy-turbulence state. (b) The backward-facing step (BFS) flow model in which a recirculation zone dominates the turbulence near the edge. The "fingerprints" of these two models on the flow statistics at the edge are shown in Table 1. The thick arrows indicate expected mean flow streamline while the thin arrows indicate the local velocity. The dashed line indicates the free-shear interface delineating a potential recirculation zone. Variables are: h_c, canopy height; z, height from the ground; and $\bar{u}$, mean longitudinal velocity.

sitions were quantified by changes in the so-called momentum roughness length (z_{om}), but rarely considered the explicit vertical geometry (or morphology). Transitions from a tall-forested canopy with a canopy height (h_c) on the order of 10 m to a forest clearing with a vegetated cover height on the order of 10 cm cannot ignore the vertical dimension imposed by the forested canopy on the bulk flow near the edge.

Over the past decade, a number of field and wind tunnel experiments considered the two-dimensional aspects of this problem for flows originating from a clearing into a forest (e.g., Irvine et al. 1997, Morse et al. 2002), mainly for windbreak applications. A less-studied problem is when the flow originates from a tall forest into a clearing (Judd et al. 1996). The mean velocity adjustments, reviewed in Lee (2000), and analytically predicted in Belcher et al. (2003) divide the flow over the clearing into three regions: (1) an exit region, in which the mean flow maintains its state as it exits from the forest edge, particularly the inflection point near the canopy top that sustains the Kelvin-Helmholtz (KH) instabilities (Judd et al. 1996, Lee 2000, Belcher et al. 2003); (2) a mixing zone, in which the KH instabilities "self-destruct" and smooth out the mean velocity profile (Lee 2000), thereby generating attached eddies to the ground; (3) a re-equilibration zone, in which the mean velocity profile is fully equilibrated with the new surface. Early experiments found that in an open field downwind of a coniferous forest, the mean velocity logarithmic profile was established at some $5h_c$ from the edge (Raynor 1971).

Here we argue that this conceptual framework, especially in the exit region, may not be general near tall and dense forest edges. For densely forested canopies, the flow may actually share several attributes with the so-called backward-facing step (BFS) flow schematically shown in Fig. 1 and qualitatively compared with exit flow predictions in Table 1. As early as 1987, a wind tunnel study already proposed that the wind pattern across a forest clearing can be temporally decomposed into "direct through-flow" (or exit flow) and "recirculating flow" (Raupach et al. 1987). In the case of a through-flow, the streamlines across the edge must be oriented with the above canopy streamlines. However, for a recirculating flow, the onset of a standing vortex within the clearing leads to a reverse flow near the ground (Raupach et al. 1987). In fact, as early as 1975, cinematic observations using multiple smoke plumes in an isolated pine forest clearing (about 10×80 m) already documented that the flow can be decomposed into rotor-like and through-flow periods (Bergen 1975). Hence, it is reasonable that the mean velocity profile at the edge can be constructed as some weighted average between these two "canonical" profiles depending on their time fraction and their relative contribution to the mean momentum equation, but the turbulent statistics that characterize this transition have not been investigated in a field setting.

Note that around the edge, the exit flow and the BFS conceptual models differ mostly in the zone bounded by the ground and h_c (Fig. 1, Table 1), the subject of this study. The exit flow model assumes that a quiet zone sets up in which the flow retains its canopy turbulence coherency in this region. We propose that this "quiet" zone shares some attributes with exit canopy turbulence but is intermittently perturbed by a recirculation pattern shown in Fig. 1 analogous to BFS flow. The intermittency in this recirculation zone is necessary to distinguish it from a continuous rotor-like circulation. Secondary recirculation zones at the clearing-edge corner are also possible and have been documented in open channel BFS studies (Simpson 1989). The rationale for a BFS analogy is that for cases in which the canopy leaf area density is sufficiently high, the mean velocity inside the forested canopy is "damped" as the transition from tall forests to a clearing progress. In the limit when the forest canopy is enough dense to resemble an impervious structure, the flow must resemble a BFS setup. The statistical properties of turbulence for BFS flows have been studied extensively in hydraulic engineering over the past two decades (Armali et al. 1983, Nakagawa and Nezu 1987, Simpson 1989, Chun and Sung 1998, Scarano et al. 1999, Spazzini et al. 2001, Kostas et al. 2002, Piirto et al. 2003, Dejoan and Leschziner 2004, Furuichi et al. 2004, Schram et al. 2004, Nezu 2005, Sheu and Rani 2006) and their mean flow properties include (Fig. 1):

1) An approximate boundary layer flow upstream from the drop structure.

2) A perturbed free shear interface that develops between the drop structure and the ground beyond the drop structure. This free shear interface extends horizontally some 5–10 h_c.

3) A recirculation zone, absent from the exit flow model, that dominates the structure of turbulence below this free shear interface. A secondary circulation zone at the corner has also been observed in some cases.

4) A reattachment zone followed by a re-equilibration zone to the new surface.

Because of the finite porosity, it is likely that the structure of turbulence near a forest edge experiences both flow types: an exit flow from the forest 'punctuated' by intermittent and highly unstable re-circulation zones (Bergen 1975) induced by a BFS like phenomenon. Whether this intermittent and unstable recirculation is significant to impact the mean momentum balance and the spectral properties of the velocity has not been explored in the field and will depend on a large number of factors including the leaf area density (Flesch and Wilson 1999), the forest canopy height, the upstream velocity, and adiabatic effects (Morse et al. 2002).

Naturally, exploring all these simultaneous effects are well beyond the scope of a single field study. The compass of this work is to investigate how a forest edge, situated at the interface between a tall pine canopy ($h_c =$ 18 m) with leaf area index (LAI) in excess of 4.5 m^2/m^2 (i.e., a dense canopy) and a grass-covered forest clearing (grass height, h_g, ~10 cm over the course of the measurement period), modifies the structure of turbulence from its near-equilibrium state in reference to the state above the grass surface (measured at 12 h_c from the forest edge and is much less contaminated by direct edge effects). In particular, we seek to explore whether there is some evidence that the edge experiences an intermittent re-circulation regime consistent with the BFS analogy and whether a BFS-like circulation can be significant to impact terms in the mean longitudinal and vertical momentum balance. For reference, we contrast several such terms in Table 1 for classical canopy "exit flow" with no adjustments and BFS-like flow. These statistics form the basis for identifying ("fingerprinting") BFS flow signatures at the edge.

TABLE 1. Comparison between canonical flow properties of backward-facing step (BFS) and exit flow near the ground of a tall forest edge.

Flow variable	BFS	Exit flow model
$\bar{w}$	+	~0 or −
$\partial\bar{w}/\partial z$	+	−
$\partial\bar{u}/\partial x$	−	~0
$\partial\bar{u}/\partial z$	−	+ (possibly − if a secondary maximum occurs inside the canopy)
$\overline{u'w'}$	+	− (possibly + if a secondary wind maximum occurs inside the canopy)
$\partial\bar{w}/\partial x$	+	~0

Notes: This assumes that no secondary mean wind maximum occurs inside the canopy as the flow progresses from the forest into a clearing (see also Fig. 1). Here "+" denotes a positive quantity, and "−" denotes negative.

For convenience, the experimental results are presented as a contrast between the flow statistics near the forest edge (i.e., highly disturbed by the edge) and their counterpart at the same measurement height above the grass surface some 12 h_c away from the edge (i.e., a reference representing a quasi-equilibrated flow state with the grass surface, though not fully equilibrated as we illustrate later). Because of natural variations in wind directions, this setup also permits us to explore some aspects of how turbulence statistics are modified by the edge for wind conditions originating from the clearing into the forest.

EXPERIMENT

The experimental site is a grass-covered forest clearing (Fig. 2a) situated at the Blackwood Division of the Duke Forest in Orange County, near Durham, North Carolina, USA (35°58′16″ N, 79°5′24″ W, elevation 163 m). The long-term mean annual temperature and precipitation are 15.5°C and 1100 mm, respectively.

The forest clearing is approximately 480 × 305 m (see Fig. 2a), dominated by the C_3 grass *Festuca arundinacea* Shreb., and surrounded by loblolly pine [*Pinus taeda* L.] forest. The site was burned in 1979 and is annually harvested during the summer for hay according to local practices. Long-term CO_2 flux measurements at the

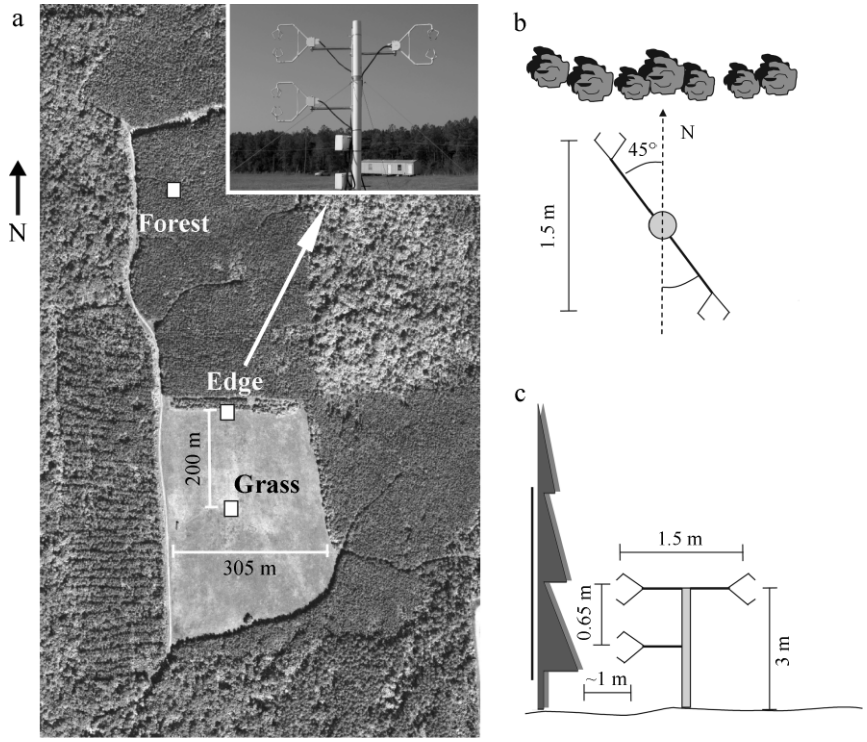

FIG. 2. (a) Aerial view of the grass-covered forest clearing and the adjacent pine forest. The location of the central grass mast, the pine forest tower, the edge mast, and (inset) a picture of the three sonic anemometer configurations at the edge are shown. (b) The plan and (c) side views of the experimental setup are shown. The approximate 1-m planar distance shown in the side view is from the center of the sonic anemometer head to the crown of the nearest tree.

central grass tower commenced in 2001 as part of a long-term flux monitoring initiative known as *Ameriflux* (Baldocchi et al. 2001). A CSAT3 sonic anemometer (Campbell Scientific, Logan, Utah, USA) is situated at 3 m above the ground surface and is used to record the three-component velocity and virtual temperature. The grass height ranges from 0.1 m following harvesting to 0.5 m or higher during well-watered periods in the growing season (Novick et al. 2004).

The forest stand, situated at the northerly edge of the grass field, is a uniformly planted (in 1983) loblolly pine forest extending some 300–600 m in the east-west direction and 1000 m in the south–north direction. Canopy height averaged 18 m at the time of the experiment. The subcanopy is densely populated with several woody species including *Liquidambar styraciflua* L., *Acer rubrum* L., *Ulmus alata*, and *Cornus florida* L. (Stoy et al. 2005, Juang et al. 2006). Thus, leaf area is distributed throughout the canopy volume and is not exclusively concentrated near the canopy top. A CSAT 3 sonic anemometer was situated at 22.6 m above the forest floor to measure the velocity components and virtual temperature above the canopy. The mean flow properties, second-order moments, and the overall structure of turbulence inside this forested stand have been extensively studied (Katul and Albertson 1998, Katul and Chang 1999, Siqueira and Katul 2002).

The measurement period extended from 14 October until 11 November 2005. To measure as many terms as possible in the mean momentum balance, an array of three sonic anemometers (see the photograph in Fig. 2) was positioned at the forest edge. Two of the anemometers were facing the edge. One of these anemometers was placed at $z = 3$ m (the same height of the sonic anemometer of the grass clearing) and the other was placed at $z = 2.35$ m, while the third anemometer was positioned at $z = 3$ m but facing the clearing. A tilt angle of about 45° from the north–south direction was applied to the arms of the sonic anemometers to avoid mutual interference in the northerly direction. The array configuration was designed to measure horizontal and vertical gradients when the mean wind direction (WD) varied from −180° (southerly wind, from the clearing into forest) to +50° (taking 0° to be northerly wind, from the forest into the clearing, and 90° to refer to winds from due east). Mean wind directions from the west and southwest (i.e., WD $\in$ [+50° to +150°]) were "contaminated" by tower distortions and sonic anemometer mutual shadowing, though these directions rarely occurred in comparison with other mean wind directions during the measurement period (Fig. 3). Horizontal and vertical gradients in all the flow statistics were computed with respect to anemometer separation distances of 1.5 m and 0.65 m, respectively (primarily when the wind

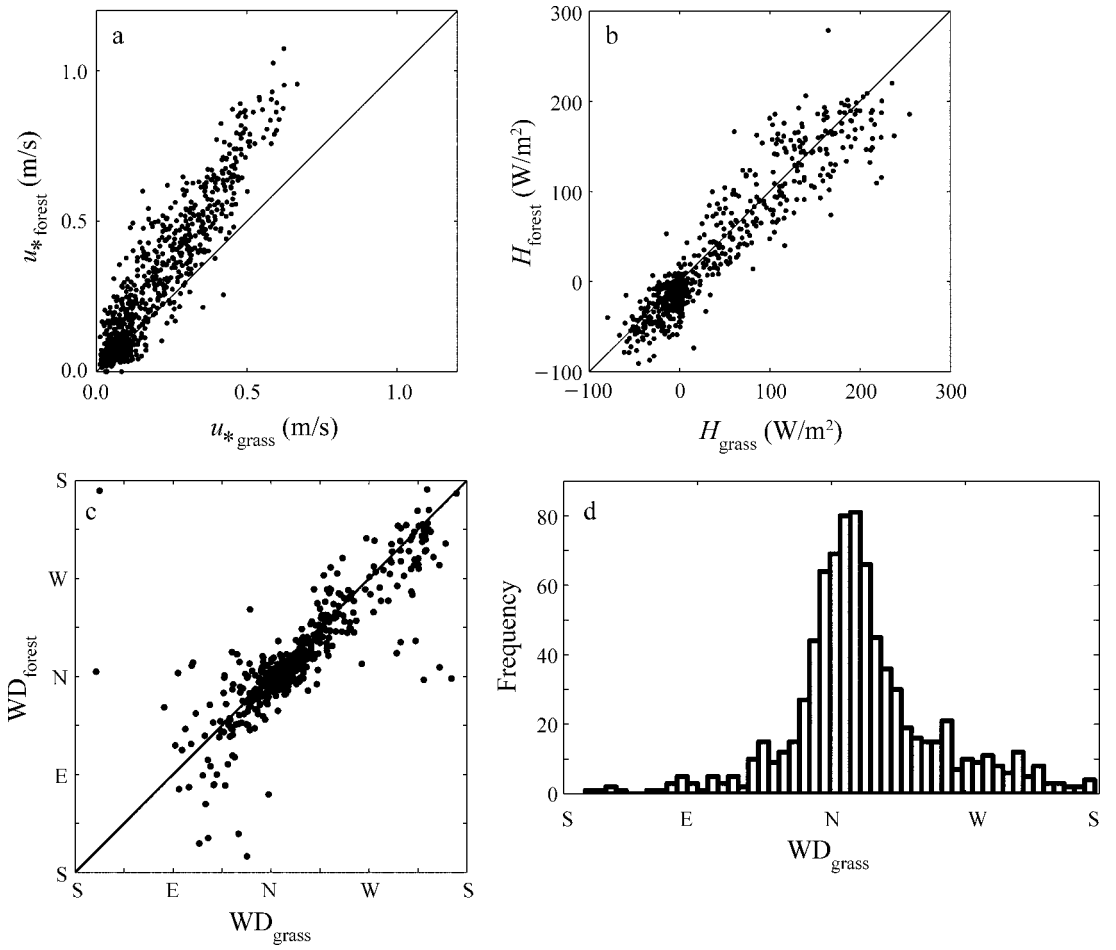

FIG. 3. Comparisons between (a) friction velocity (u_*), (b) sensible heat flux (H), and (c) wind direction (WD) measured at the center of the grass clearing (grass tower) and at the forest during the study period, and (d) the histogram of wind directions during the same period. Note that the dominant wind direction is approximately from the north (i.e., from the forest into the grass clearing).

direction was from north to south or south to north). The time series from all the sonic anemometers were sampled at 10 Hz, divided into 30-minute runs for post-processing, and all the key statistics for each run were then computed.

During the measurement period, we found that the sensible heat flux (H) from the grass clearing and from the pine forest were comparable; however, the friction velocity (u_*) was 40% smaller at the clearing when compared to the pine forest (Fig. 3a, b). Hence, in a first order analysis, the flow into the forest edge experiences a significant "jump" in the mean momentum flux but no concomitant change in the sensible heat flux. The wind directions measured at the pine forest and central grass towers were consistent as shown also in Fig. 3c when the mean wind speed was larger than 1 m/s at the grass tower.

Throughout, we use both index and meteorological notations as follows: x_1 or x, x_2 or y, x_3 or z are the longitudinal, lateral, and vertical directions, respectively, u_1 or u, u_2 or v, u_3 or w are the instantaneous velocities along x_1, x_2, and x_3; t is time, T is virtual temperature, the overbar represents time-averaging over 30 minutes, and primed quantities denote instantaneous turbulent excursions from the time-averaged state. For each run, the measured velocity time series was rotated such that x_1 is aligned along the mean wind direction (i.e., $\bar{v} = 0$). No vertical rotation was employed because of the need to compute flow statistics such as $\partial\bar{w}/\partial z$. The variance of an arbitrary flow variable s is defined as $\sigma_s^2 = \overline{s'^2}$ and its vertical turbulent flux is $\overline{w's'}$. Hereafter, we refer to the tower locations at the center of the grass clearing and the pine forest as grass tower and pine tower, respectively.

RESULTS AND DISCUSSION

The effects of the forest edge on the structure of turbulence near the grass–forest interface are first explored by contrasting the bulk flow statistics collected

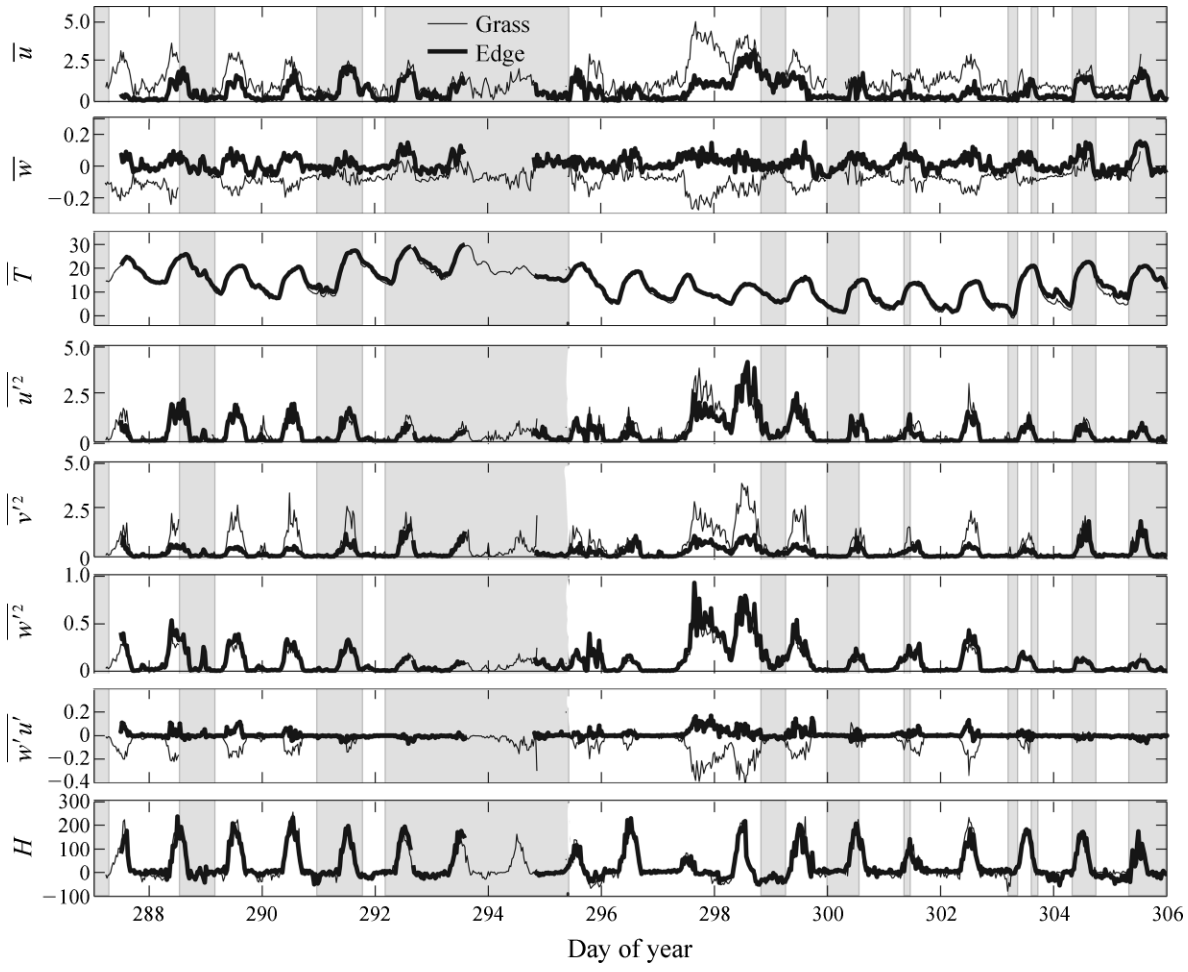

FIG. 4. Time series comparisons between the flow statistics at the forest edge and the flow statistics in the clearing at $z = 3$ m, where day 1 is 1 January. The statistics compared include mean longitudinal $\bar{u}$ (m/s), and vertical velocity $\bar{w}$ (m/s), mean virtual temperature $\overline{T}$ (°C), longitudinal velocity variance $\overline{u'^2}$ (m^2/s^2), lateral velocity variance $\overline{v'^2}$ (m^2/s^2), vertical velocity variance $\overline{w'^2}$ (m^2/s^2), mean momentum flux $\overline{w'u'}$ (m^2/s^2), and sensible heat flux H (W/m^2). Flow originates from the forest into the clearing under northerly wind directions $\in [0 \pm 45°]$. Data shown in gray shaded areas are for directions other than northerly.

at the edge with the flow statistics collected at the grass tower for two clusters of wind directions: north (i.e., from the forest into the clearing direction within ±45°) and the remaining wind directions. We then proceed to explore the "fingerprints" of the intermittent BFS-like circulation in the velocity statistics relevant to the mean momentum balance as in Table 1. The implications of the experimental findings to closure approximations are then discussed and typical mixing length scales are investigated using spectral analysis.

Comparison between the flow at the edge and the flow in the clearing

In Fig. 4, the time series of key flow statistics measured by the sonic anemometers at the edge and at grass tower are presented for the entire experiment duration. The following salient features can be noted:

1) The $\bar{u}$ at the edge is much smaller than $\bar{u}$ at the grass tower for almost all the runs, as expected.

2) The $\bar{w}$ at the edge is positive on average, but is negative at the grass tower (consistent with the BFS like circulation in Fig. 1).

3) The $\bar{T}$ differences between the two tower stations are minor, at least when this difference is compared to the diurnal variation.

4) The differences between measured $\overline{u'^2}$ and $\overline{w'^2}$ at the two stations are surprisingly small when compared to differences in $\overline{v'^2}$, though not for the entire record duration.

5) The momentum flux $\overline{w'u'}$ is negative at the grass tower (as expected in a turbulent boundary layer) but is often positive and large at the forest edge (especially during periods of high $\bar{u}$) hinting at some BFS-like recirculation (Fig. 1).

6) The sensible heat flux differences between the two towers are minor, which is expected given the similarity in sensible heat fluxes between the pine forest and grass surface (Fig. 2).

Upon clustering the data in two wind directions (northerly and all other directions), we find that the differences in $\bar{u}$ and $\overline{v'^2}$ largely occur when the flow originates from the forest into the clearing as shown in Fig. 5a, c. Surprisingly, a 1:1 agreement between the flow statistics at the edge and in the center for $\overline{u'^2}$ and $\overline{w'^2}$ (Fig. 5b, d) was recorded for all wind conditions, suggesting that the forest edge played a minor role in modulating these two quantities when compared to $\overline{v'^2}$.

One explanation for the $\overline{u'^2}$ similarity at the two tower sites may be attributed to large-scale "inactive eddies" originating from the outer layer and contributing to longitudinal velocity variance at these two locations (Katul et al. 1996, Katul and Chu 1998). This explanation does not contradict the $\overline{w'u'}$ dissimilarities recorded in the time series, as the inactive eddy motion by definition does not contribute to the momentum flux. However, this argument cannot explain similarities in the measured $\overline{w'^2}$ at these two sites because $\overline{w'^2}$ is also much less impacted by the inactive eddy motion (Katul and Chu 1998). We return to this point in the spectral analysis section. The most notable "edge effect" was manifested in the $\overline{v'^2}$, which was reduced by almost a factor of three relative to its grass tower counterpart for northerly wind conditions. To explain why $\overline{v'^2}$ does not adjust as rapidly as $\overline{u'^2}$ and $\overline{w'^2}$, consider its budget equation, given by

$$\frac{\partial \overline{v'^2}}{\partial t} + \overline{u}_j \frac{\partial \overline{v'^2}}{\partial x_j} = \underbrace{2\overline{v'u'_j}\frac{\partial \overline{v}}{\partial x_j}}_{[1]} \underbrace{- 2\frac{\partial \overline{u'_j v'^2}}{\partial x_j}}_{[2]} + \underbrace{\left[-\left(\frac{2}{\rho}\right)\frac{\partial \overline{v'p'}}{\partial y} + \left(\frac{2}{\rho}\right)\overline{p'\frac{\partial v'}{\partial y}} \right]}_{[3]} \underbrace{- 2\upsilon_m \frac{\overline{\partial v'^2}}{\partial x_j}}_{[4]}$$

$$\frac{D\overline{v'^2}}{Dt} = [1] + [2] + [3] + [4] \qquad (1)$$

where $D(\cdot)/Dt$ is the material derivative, υ_m is the kinematic molecular air viscosity, ρ is the mean air density, and p' is the turbulent static pressure fluctuation. Term [1] represents the variance production (extracting energy from the mean flow), term [2] is turbulent transport, term [3] is pressure transport and redistribution, and term [4] is viscous dissipation. By virtue of the coordinate system, $\bar{v} = 0$, and the lateral symmetry in the experimental setup for northerly wind conditions leads to $\partial(\cdot)/\partial y = 0$ both inside the forest and above the clearing. This setup means that the turbulent transport term (i.e., term [2]) becomes the primary mechanism that can increase $D\overline{v'^2}/Dt$ as the flow progresses from within the forest into the clearing. The fact that the pressure re-distribution term and production terms are absent here can explain why $\overline{v'^2}$ adjusts much more slowly when compared to $\overline{u'^2}$ and $\overline{w'^2}$.

The mean momentum balance equation at the forest edge

For a stationary high Reynolds number flow that is homogeneous along the lateral direction, the three sonic anemometer array positioned at the edge permitted us to estimate key terms in the mean continuity,

$$\frac{\partial \bar{u}}{\partial x} + \frac{\partial \bar{w}}{\partial z} = 0 \qquad (2)$$

and in the longitudinal and vertical mean momentum balances, given by

x direction:

$$\bar{u}\frac{\partial \bar{u}}{\partial x} + \bar{w}\frac{\partial \bar{u}}{\partial z} + \frac{\partial \overline{u'w'}}{\partial z} + \frac{\partial \overline{u'u'}}{\partial x} \approx -\frac{1}{\rho}\frac{\partial \bar{p}}{\partial x}$$

z direction:

$$\bar{u}\frac{\partial \bar{w}}{\partial x} + \bar{w}\frac{\partial \bar{w}}{\partial z} + \frac{\partial \overline{u'w'}}{\partial z} + \frac{\partial \overline{w'w'}}{\partial z} \approx -\frac{1}{\rho}\frac{\partial \bar{p}}{\partial z}. \qquad (3)$$

Except for the turbulent pressure gradients, all terms on the left-hand side of Eqs. 2 and 3 can be measured near the edge, and are shown in Figs. 6 and 7 as a function of wind direction. Because our focus is on northerly wind directions (WD ≈ 0 here is the forest-to-clearing), data not directly relevant to these directions is shaded; for completeness we present the entire record. A number of salient features are evident from these two figures (see also Table 1):

1) For forest-to-clearing wind directions, the predominantly negative $\partial\bar{u}/\partial z$ close to the forest–clearing edge is consistent with the BFS analogy (see Fig. 1 and Table 1). A $\partial\bar{u}/\partial z < 0$ is also consistent with the exit flow model if a secondary maximum in mean velocity exists inside the canopy (Shaw 1977, Wilson and Shaw 1977). Note that for clearing-to-forest wind directions (WD ≈ -180), $\partial\bar{u}/\partial z > 0$, compatible with standard boundary layer flows over the grass surface and lending further confidence in the gradient measurements.

2) For forest-to-clearing wind directions, $\partial\bar{u}/\partial x$ is mostly negative, which is in agreement with a BFS flow (Table 1). Again, note that for the clearing-to-forest wind direction (WD ≈ -180), $\partial\bar{u}/\partial x > 0$ this lends additional confidence in these gradient measurements). For the BFS analogy, a simple order of magnitude suggests that the distance at which sign reversal in the mean flow (i.e., $\bar{u} < 0$) is expected is $\bar{u}/(\partial\bar{u}/\partial x) \sim 1/0.1 \sim 10$ m or within h_c from the forest edge. In this calculation, $\bar{u}$ and $\partial\bar{u}/\partial x$ were determined by ensemble averaging the northerly wind direction data in Figs. 5 and 6. This horizontal distance is similar to several flow visualization experiments on BFS in open-channel hydraulics (Simpson 1989) and smoke release experiments in Bergen (1975). The latter study reported intermittent recirculating eddies between h_c and 2.7 h_c (McNaughton 1989) (i.e., horizontal distance of the same order of magnitude as h_c).

3) For forest-to-clearing wind directions, both $\bar{w}$ (see unshaded areas in Fig. 4) and $\partial\bar{w}/\partial z$ (Fig. 6d) were

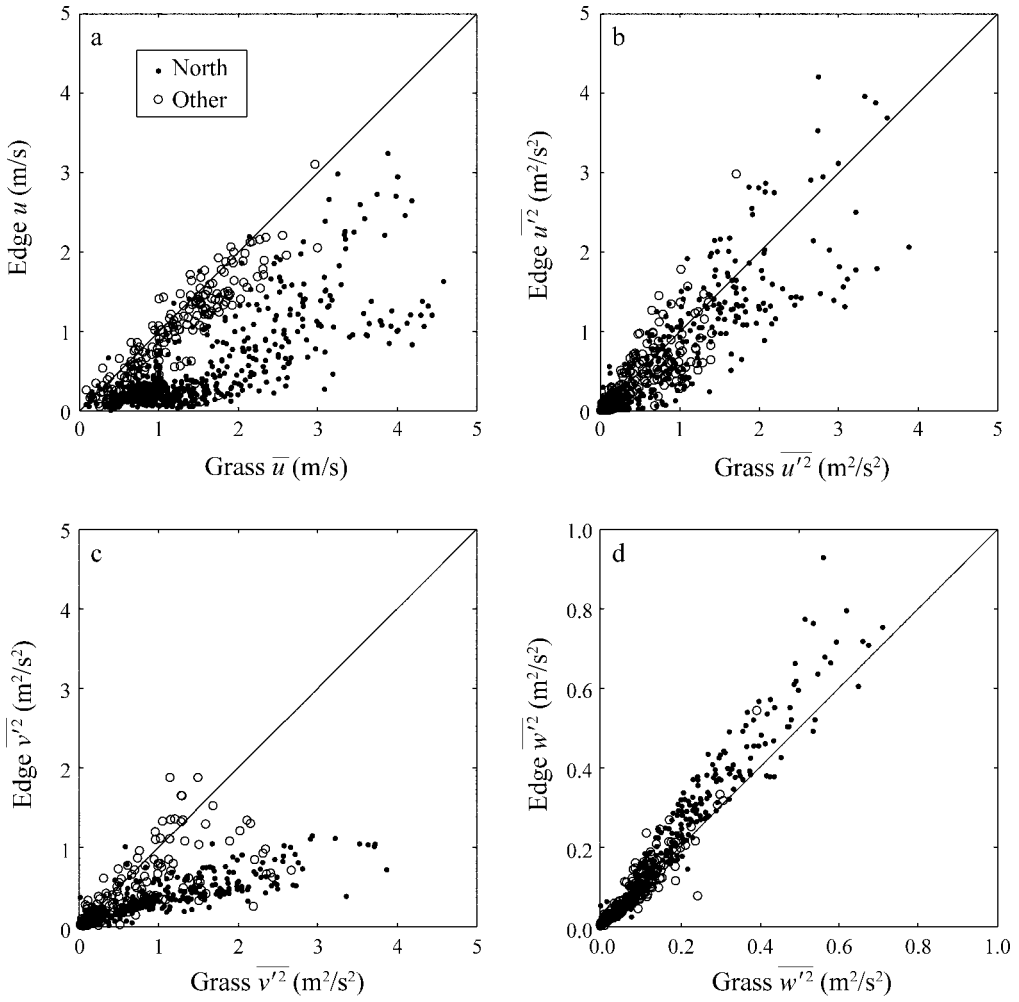

FIG. 5. Comparison between the flow statistics at the edge vs. the central grass tower for (a) the mean longitudinal velocity ($\bar{u}$), (b) the longitudinal velocity variance ($\overline{u'^2}$), (c) the lateral velocity variance ($\overline{v'^2}$), and (d) the vertical velocity variance ($\overline{w'^2}$). The 1:1 line is shown for reference. The data are clustered based on wind direction, with northerly wind directions (flow from forest to clearing) in solid circles and all other directions in open circles. Note the scale difference (on both axes) for the $\overline{w'^2}$ comparisons.

positive, again pointing to a BFS-like circulation (see Table 1). For all other wind directions, $\partial\bar{w}/\partial z$ was small but consistently positive. This consistent positive $\partial\bar{w}/\partial z$ is not unexpected given that $\bar{w} = 0$ at the ground. Recall that in a standard exit flow scenario, the mean velocity turns downward to fill out the clearing immediately after its upstream edge (Fig. 1; see also Fig. 10 in Belcher et al. 2003), thereby resulting in a negative $\bar{w}$. When combined with $\bar{w} = 0$ at the ground, it leads to a $\partial\bar{w}/\partial z < 0$ (see Table 1).

4) For forest-to-clearing wind directions, $\partial\bar{w}/\partial x > 0$, again suggesting that the increase in $\bar{w}$ is likely to be linked with upward mean flow consistent with the BFS analogy (Fig. 6b; Table 1).

5) For forest-to-clearing wind directions, the ensemble-averaged $\partial\bar{u}/\partial x \approx -\partial\bar{w}/\partial z$ as predicted by the mean continuity equation (Fig. 6a, d) thereby lending further confidence in these velocity gradient measurements. In particular, we find that $\partial\bar{u}/\partial x \approx -\partial\bar{w}/\partial z$ is well satisfied for large events (i.e., when $\partial\bar{u}/\partial x \approx -0.2$ s^{-1}, $-\partial\bar{w}/\partial z \approx 0.2$ s^{-1}), suggesting that these agreements are not fortuitous artifacts of sonic anemometer biases or electronics. For the other wind directions (shaded regions), care must be used in interpreting the continuity equation as distances between the three sonic anemometers becomes highly sensitive to wind direction, and the lateral direction is no longer homogeneous.

6) With regard to the terms in the mean longitudinal momentum balance (Fig. 7) and for forest-to-clearing wind directions, significant $\partial\overline{u'w'}/\partial z > 0$ (i.e., positive change in momentum flux with height) was measured (panel f), again consistent with the BFS analogy. Note that for clearing-to-forest wind directions, the vertical gradients in the momentum flux $\partial\overline{u'w'}/\partial z$ are negligible, suggesting that a near-constant stress assumption is reasonable even in the vicinity of the edge. As in the

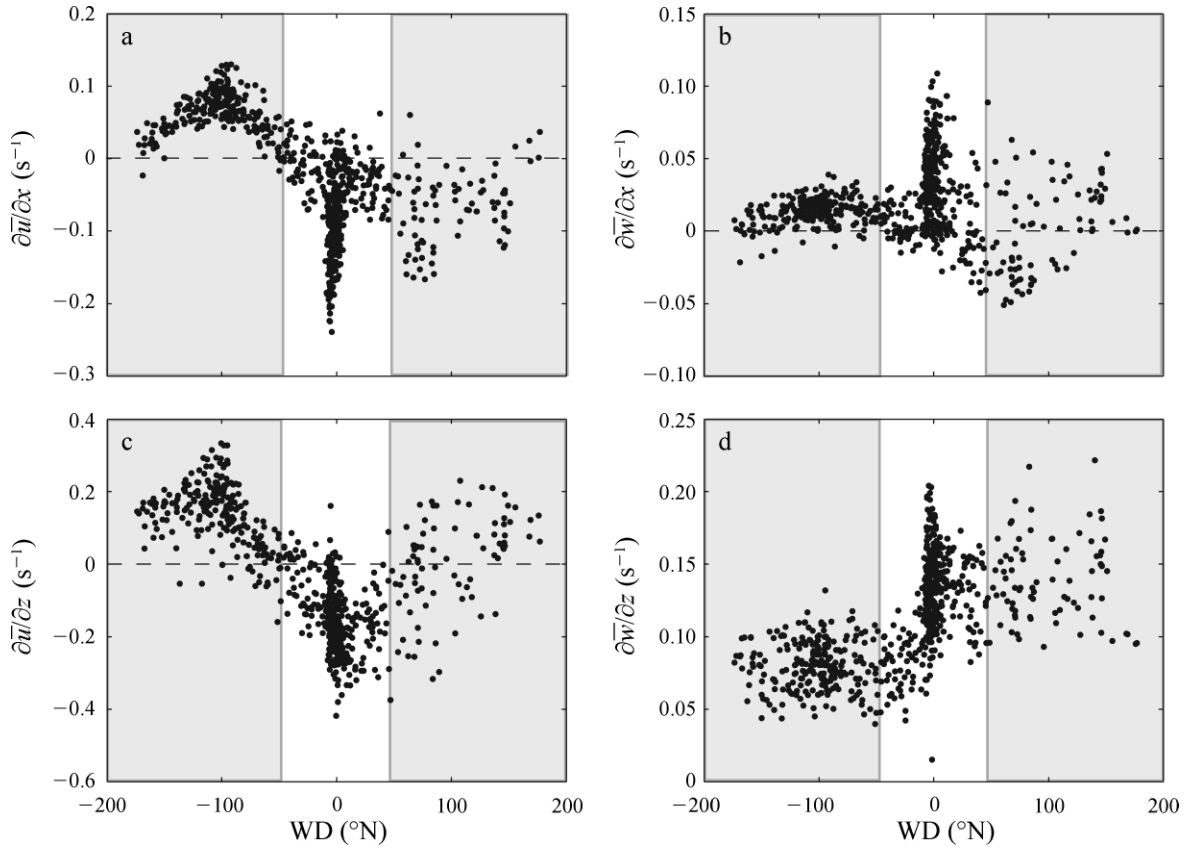

FIG. 6. Variations of (a) $\partial\bar{u}/\partial x$, (b) $\partial\bar{w}/\partial x$, (c) $\partial\bar{u}/\partial z$, and (d) $\partial\bar{w}/\partial z$ with the mean wind direction (WD) evaluated at the center of the field. Flow originates from the forest into the clearing under northerly wind directions $\in [0 \pm 45°]$. Data shown in gray shaded areas are for all other directions. Note that tower distortions and sonic anemometer overshadowing are significant for WD $\in$ [50, 150].

$\partial\bar{u}/\partial z < 0$ case, a $\partial\overline{u'w'}/\partial z > 0$ for northerly directions may be consistent with an exit flow condition if a secondary-wind maximum exists inside the canopy (Shaw 1977, Wilson and Shaw 1977). We explore this point later and demonstrate that conditions promoting secondary maxima in the forest act against the BFS flow. Specifically, the occurrence of a BFS-like circulation and secondary maxima require almost opposite upwind shear stress conditions (at least for this site).

7) For forest-to-clearing wind directions, a large and positive $\partial\overline{w'^2}/\partial z$ was measured (Fig. 7f), consistent with both the exit flow model and BFS, while for the clearing-to-forest wind direction, the $|\partial\overline{w'^2}/\partial z| \approx 0$ consistent with standard near-neutral surface layer analysis and the near-zero $\partial\overline{u'w'}/\partial z \approx 0$ term.

8) For forest-to-clearing wind direction, measured $\partial\overline{w'^2}/\partial x < 0$ (Fig. 7b) and this gradient cannot be consistent with the exit flow model (even in the presence of a secondary mean wind maximum). In fact, other experiments (Flesch and Wilson 1999) reported an increase in their turbulent kinetic energy with distance from a sparse forest edge after demonstrating that rotor-like circulation is absent in their data. For the clearing-to-forest wind direction, again note that $|\partial\overline{w'^2}/\partial x| \approx 0$ and remains consistent with a near-neutral atmospheric surface layer.

9) The longitudinal and vertical gradients of $\overline{u'^2}$ in Fig. 7a, d confirm the findings for the $\overline{w'^2}$ analysis when considered in the context of Table 1. Again, note that for clearing-to-forest wind direction, $|\partial\overline{u'^2}/\partial x| \approx 0$ consistent with a near-neutral atmospheric surface layer.

10) Among all the terms in the longitudinal mean momentum balance, $|\partial\overline{u'w'}/\partial x|$ was the smallest for forest into clearing wind directions (Fig. 7c).

As earlier stated, the fact that measured $\partial\bar{u}/\partial z < 0$, $\partial\bar{w}/\partial z > 0$, and $\overline{u'w'} > 0$ can be explained by an exit flow model with a secondary maximum in the mean velocity profile (Shaw 1977, Wilson and Shaw 1977, Katul and Chang 1999, Morse et al. 2002). To investigate this point further, we consider the measured profiles in Fig. 8 collected inside the same pine canopy (Katul and Albertson 1998, Katul and Chang 1999) albeit at different dates. The ensemble of these profiles do suggest a weak $\partial\bar{u}/\partial z < 0$, $\partial\bar{w}/\partial z > 0$, and $\overline{u'w'} > 0$ at $z = 4.15$ m (lowest measurement level), a level comparable to the $z =$ 3 m used for the forest edge measurements. However, these data also suggest that $\bar{w}$ appears to be mildly negative, and $\partial\bar{u}/\partial z$ becomes increasingly positive with

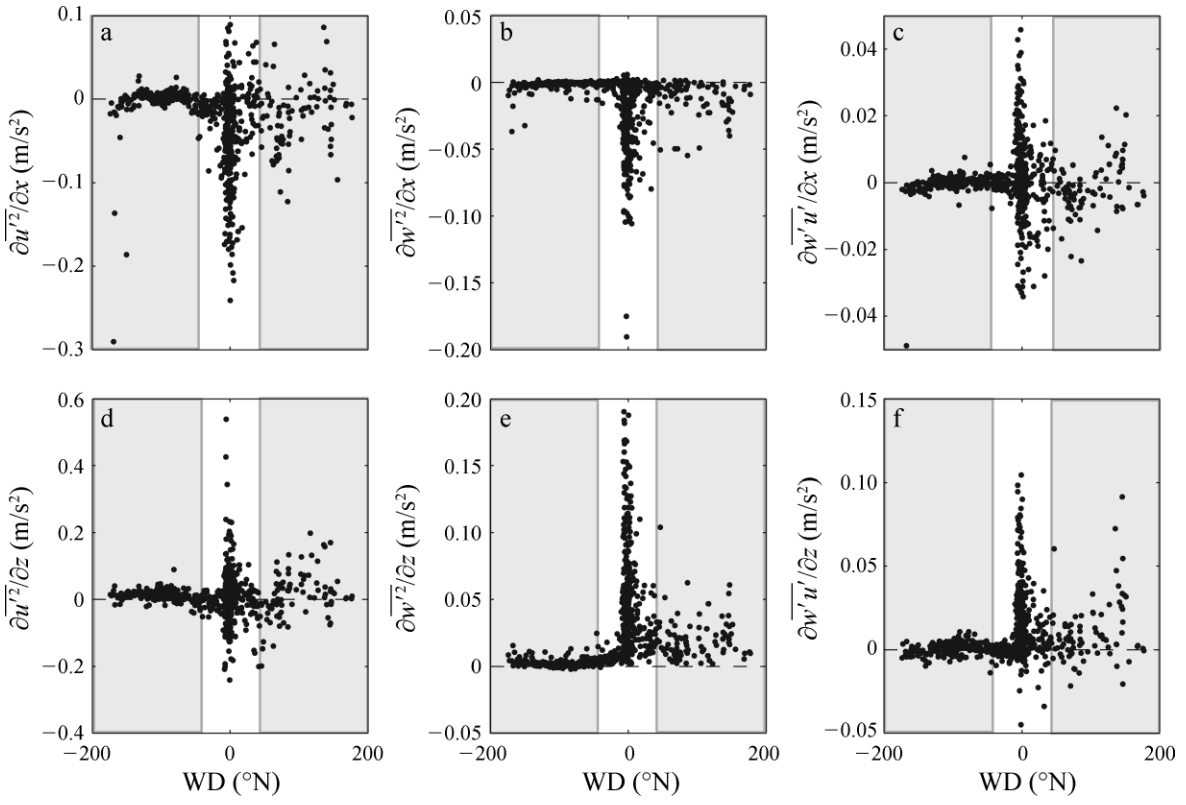

FIG. 7. Same as Fig. 5, but for the second-order statistics: (a) $\partial\overline{u'^2}/\partial x$, (b) $\partial\overline{w'^2}/\partial x$, (c) $\partial\overline{w'u'}/\partial x$, (d) $\partial\overline{u'^2}/\partial z$, (e) $\partial\overline{w'^2}/\partial z$, and (f) $\partial\overline{u'w'}/\partial z$.

increasing mean velocity above the forest canopy (u_o). If we re-computed these profiles conditioned on $u_o > 3$ m/s (also shown in Fig. 8), we find that the mean velocity profile approaches its "classical" exponential form, $|\bar{w}| \approx 0$, and $\overline{u'w'} < 0$ throughout the pine canopy. Hence, it is the classical canopy turbulence profiles with their $\partial\bar{u}/\partial z > 0$, $\bar{w} \approx 0$, and $\overline{u'w'} < 0$ properties that prevail for exit flow conditions at the edge when the upwind mean velocity is large. Recall that these strong mean wind conditions are the ones promoting intermittent recirculation at the edge in the framework of the BFS analogy.

In a BFS open-channel flow, the recirculation region is linked to the magnitude of the upstream shear stress (Nakagawa and Nezu 1987). Hence, as further (but admittedly indirect) evidence of a BFS-analogy near the forest edge, we investigate whether $\partial\bar{u}/\partial x$ becomes increasingly negative as measured friction u_* at the pine tower increases for all forest-to-clearing wind directions. From Fig. 9, it is clear that as u_* above the forest increases, $\partial\bar{u}/\partial x$ at the edge becomes increasingly negative, again consistent with the BFS patterns observed in open channel flows. Recall that a negative $\partial\bar{u}/\partial x$ is a necessary, but not sufficient, condition for a negative $\bar{u}$ in the clearing thereby setting up a recirculation zone.

Closure models for the mean momentum balance

We demonstrated that BSF-like flows are likely at the dense forest edge measured here. If a BSF-like flow exists, what are plausible closure models for the mean pressure gradients and turbulent stresses near forest edges?

The (inferred) mean pressure gradients at the forest edge

Given the difficulties in measuring the turbulent pressure gradients at the forest edge (Nieveen et al. 2001), we used Eq. 3 to estimate these terms as residuals with the cautionary comment that all measurement errors are likely to "infect" this estimate. In Fig. 10, we show the variations of $\rho^{-1}\partial\bar{p}/\partial x$ and $\rho^{-1}\partial\bar{p}/\partial z$ determined from the residuals for northerly wind directions only and analyze them with respect to the anticipated $\rho^{-1}\partial\bar{p}/\partial x$ and $\rho^{-1}\partial\bar{p}/\partial z$ determined from drag-force analogies inside the canopy. Inside the canopy, recall that

$$\left\langle \rho^{-1}\partial\bar{p}/\partial x_i \right\rangle \approx C_d a|\bar{u}|\bar{u}_i \tag{4}$$

where $\langle\cdot\rangle$ is the usual spatial averaging operator (Raupach and Shaw 1982), C_d is the canopy drag coefficient estimated by Katul and Albertson (1998) for this site to be $\approx$0.2, and $a = \mathrm{LAI}/h_c$ is the mean leaf area density. Upon regressing the estimated $\rho^{-1}\partial\bar{p}/\partial x$ and

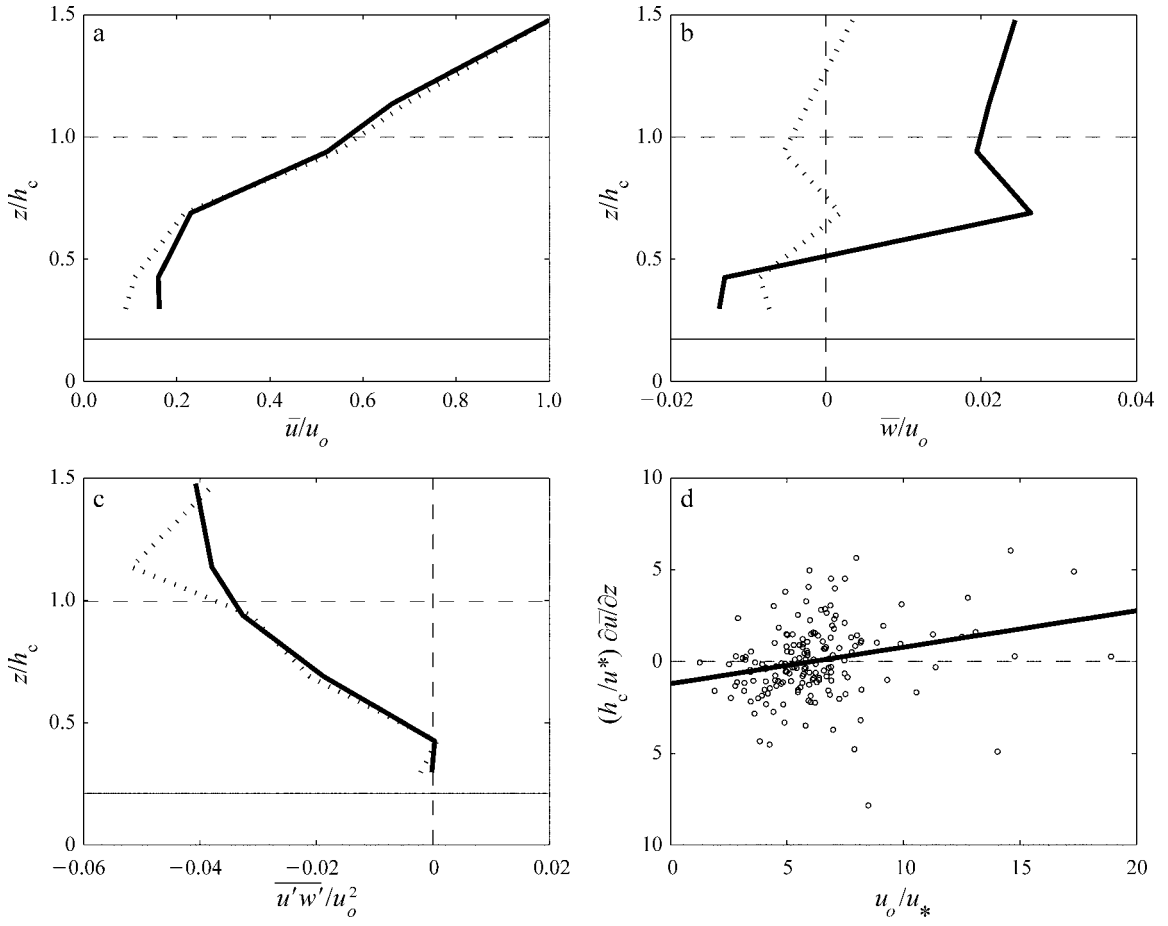

FIG. 8. Mean profiles of (a) $\bar{u}$, (b) $\bar{w}$, and (c) $\overline{u'w'}$ inside the pine forest for all the mean wind and atmospheric stability conditions (solid lines) described in Katul and Albertson (1998). The profiles for these same variables, conditioned on strong mean wind speed above the canopy ($u_o > 3$ m/s) are shown as dashed lines (not horizontal) in those panels. (d) The variation of $\partial\bar{u}/\partial z$ as a function of u_o is also presented along with the regression line for reference. In all four panels, the velocity is normalized by u_o or the friction velocity (u_*) measured above the canopy. The length scales are normalized by the mean canopy height (h_c). In panels (a)–(c), the height of the measurements conducted at the forest edge is shown as thin horizontal continuous line, and the canopy top ($z/h = 1$) is shown as a horizontal dashed line for reference. Note the shift toward "classical" dense canopy turbulence profiles for $u_o > 3$ m/s in these three panels. In panel (d), the dashed line represents the zero gradient.

$\rho^{-1}\partial\bar{p}/\partial z$ against $|\bar{u}|\bar{u}_i$, a closure model for the pressure terms can be explored. The regression slope in Fig. 10 can be interpreted as an effective $C_d a$. Based on linear regression analysis of the data in Fig. 10, we computed for the longitudinal direction a slope that is $\approx$0.051, which is in good agreement with the estimate based on $C_d \times (\mathrm{LAI}/h_c) = 0.2 \times 4.8/18 \approx 0.053$ for the pine forest. However, for the vertical direction, we found that the slope of the regression line (i.e., $C_d a$) is one order of magnitude larger than 0.053, suggesting that additional mechanisms, perhaps linked with a recirculation-induced change, must be responsible for enhancing $\rho^{-1}\partial\bar{p}/\partial z$ beyond its canopy drag value.

To assess whether the pressure gradient relationship in Fig. 10 are consistent with other direct pressure measurements conducted at similar sites, we considered the ground pressure measurements for the tussock grassland–forest interface experiment described by Nieveen et al. (2001). Using five quad-disks static pressure measurements from the clearing into the forest positioned at the ground, they found that when the flow direction is from smooth to rough (or clearing to forest), maximum pressure differences occur within the forest ($x/h_c \sim 0.6$, noting that $h_c = 25$ m in their experiment). However, when the flow transitions from rough to smooth (or forest to clearing), they found that the pressure differences between the forest and the grassland is comparatively weak, one order of magnitude smaller than the smooth-to-rough case, and occurs near the forest edge. We used their published data (their Table 2) to estimate a ground-based $\rho^{-1}\partial\bar{p}/\partial x$ at their edge as a function of $\bar{u}^2$, which was only available at their grassland for cases when their $\Delta P_{50} > 0$ (i.e., pressure difference between the disk at 100 m inside the forest and 50 m into the clearing from the edge). We used $\Delta P_{50} > 0$ at $x/h_c = 0$ because we wanted to ensure a significant

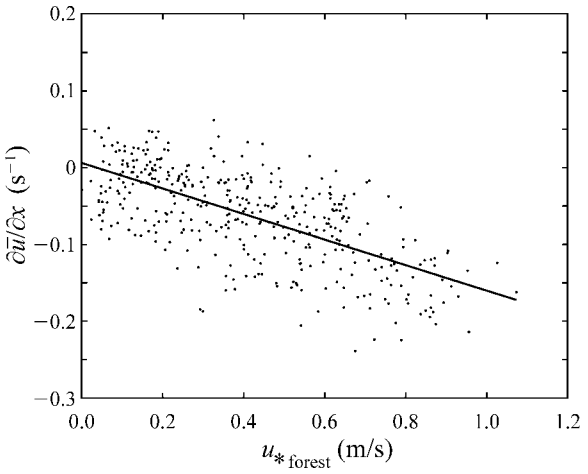

FIG. 9. The variation of $\partial\bar{u}/\partial x$ at the forest edge with u_* above the pine forest canopy for northerly wind directions (WD $\in [0 \pm 45°]$). Note that $\partial\bar{u}/\partial x$ becomes increasingly negative with increasing u_*, consistent with the BFS analogy.

re-attachment zone away from the edge during their experiment thereby eliminating other mechanisms known to influence ground pressure (e.g., adiabatic differences between the two surfaces). The overall trend in their ground pressure $-\rho^{-1}\partial\bar{p}/\partial x$, shown in Fig. 11, is consistent with our findings in Fig. 10 (top panel). Analogous findings about the importance of the term $-\rho^{-1}\partial\bar{p}/\partial x$ were observed in the numerical simulation carried out by Li et al. (1990). When taken together, these three studies unambiguously demonstrate that $-\rho^{-1}\partial\bar{p}/\partial x$, a term often neglected in Reynolds-averaged Navier-Stokes (RANS) IBL models of forest edges (e.g., Rao et al. 1974, Garratt 1990, Kaimal and Finningan 1994), plays an important role in the mean momentum balance. Furthermore, the agreement between the findings in Fig. 10a and Fig. 11b lends additional confidence to our indirect estimates of $\rho^{-1}\partial\bar{p}/\partial x$ at the edge.

Mixing length models for the Reynolds stress at the forest edge

To explore whether a single canonical mixing length l is sufficient to explain the positive $\overline{w'u'}$ from mean velocity gradients, standard first order closure principles, given by

$$\overline{u'w'} = -l^2\left|\frac{\partial\bar{u}}{\partial z}\right|\frac{\partial\bar{u}}{\partial z} \tag{5}$$

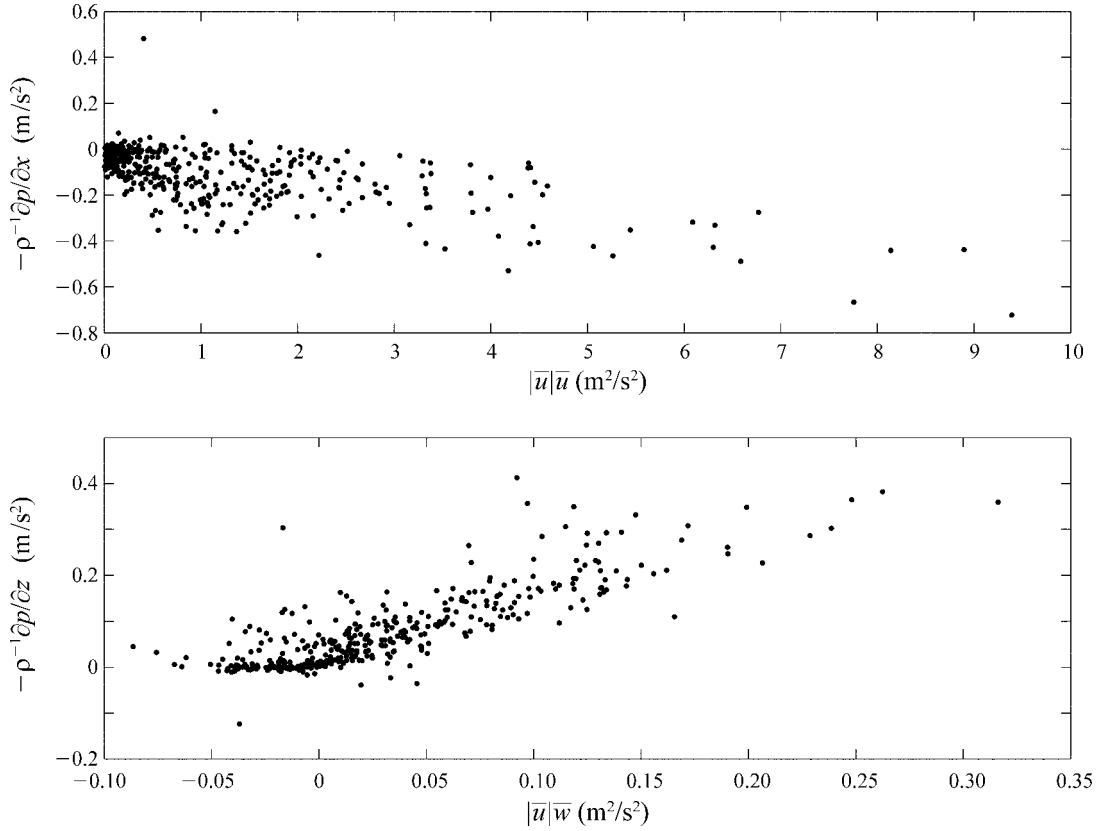

FIG. 10. The variation of $-\rho^{-1}\partial\bar{p}/\partial x$ (top) and $-\rho^{-1}\partial\bar{p}/\partial z$ (bottom) against local variations in $|\bar{u}|\bar{u}$ and $|\bar{u}|\bar{w}$, respectively, are shown at the forest edge for northerly wind directions. Note that these pressure gradients are determined as residuals from the mean momentum balance.

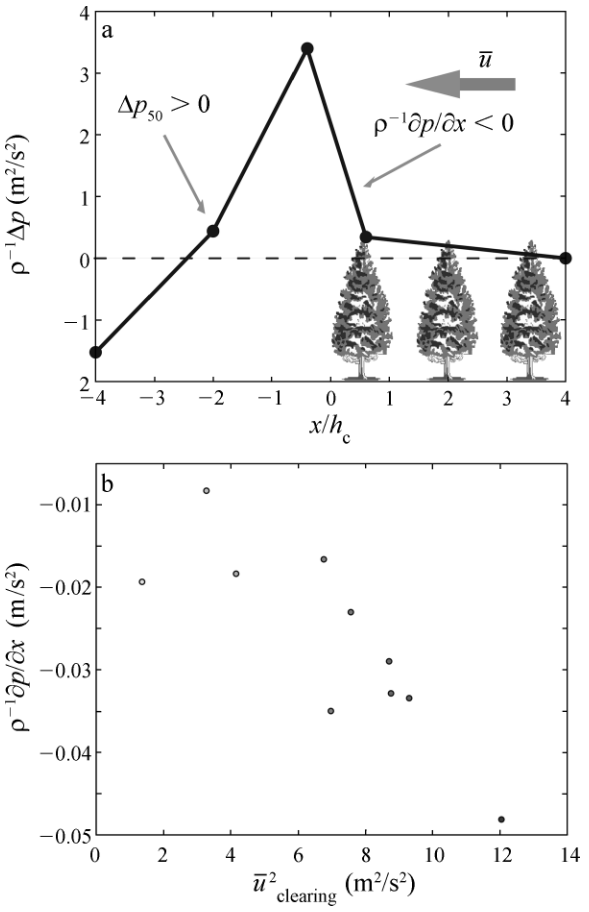

FIG. 11. (a) The measured ensemble variation of ground pressure difference Δp (referenced to the forest value) normalized by air density ρ with distance x normalized by the canopy height h_c for conditions ensuring a re-attachment zone at 50 m ($\Delta p_{50} > 0$) using data from Nieveen et al. (2001). (b) The measured variations of $-\rho^{-}\partial\bar{p}/\partial x$ at the forest-clearing edge with variations in $\bar{u}^2$ at the grass for all runs with $\Delta p > 0$ using data from Nieveen et al. (2001).

are used, where the term

$$l^2\left|\frac{\partial\bar{u}}{\partial z}\right|$$

is the effective turbulent diffusivity. We determined l^2 by regressing

$$\left|\frac{\partial\bar{u}}{\partial z}\right|\frac{\partial\bar{u}}{\partial z}$$

upon $\overline{u'w'}$ in Fig. 12 and compared these estimates to two plausible mixing length scales: (1) $k_v z$ representing a standard boundary layer mixing length, where $k_v = 0.4$ is the von Karman constant, z is the measurement height, and αh_c represents a standard canopy mixing length with $\alpha \approx 0.1$ determined for dense canopy flows in flume experiments (Poggi et al. 2004). The large scatter in Fig. 12 demonstrates a disappointing "non-uniqueness" in the mixing length. Interestingly, most of the runs appear to yield mixing lengths bounded by 0.2 h_c (=3.6 m) and $k_v z/10 \approx 0.12$ m. This result motivated us to explore, via wavelet spectra and co-spectra, the range of length scales that may contribute to the generation of positive momentum fluxes at the edge.

Spectral and co-spectral comparisons between the forest edge and the grass surface

We compared the Haar wavelet velocity spectra and co-spectra at the edge with their counterparts above the grass clearing, the latter representing a quasi-equilibrated flow with the grass surface (see Fig. 13). The choice of wavelet analysis over its Fourier counterparts are discussed elsewhere (Katul et al. 1994, 2001) and are not repeated here. We estimated the Haar wavelet wave number (K) from the sampling frequency and local $\bar{u}$ using Taylor's frozen turbulence hypothesis. Because of the need to use Taylor's hypothesis, we only considered runs with high wind speeds at the edge (squared turbulent intensity <0.25 at the edge). Fig. 13 shows a sample 54-minute run collected under a $\bar{u} = 3$ m/s measured at the grass tower and a $\bar{u} = 1.4$ m/s measured at the edge (data collected at the two towers almost simultaneously).

Not surprisingly, we found that the energetic scales in the vertical velocity spectrum (KS_w) are bounded between $k_v z$ and h_c; and that the signature of the inertial sub-range ($-2/3$ power law) commences around $z/2$, consistent with an earlier study on local isotropy at this site (Katul et al. 1997). For the longitudinal velocity energy (KS_u), we found that the energetic scales generally exceed h_c, suggesting some inactive eddy motion from the outer layer may be contributing to $\overline{u'^2}$ at both the central grass tower and the edge sites. For the lateral velocity energy, the energetic scales do not exceed h_c near the edge, again suggesting dissimilarity in

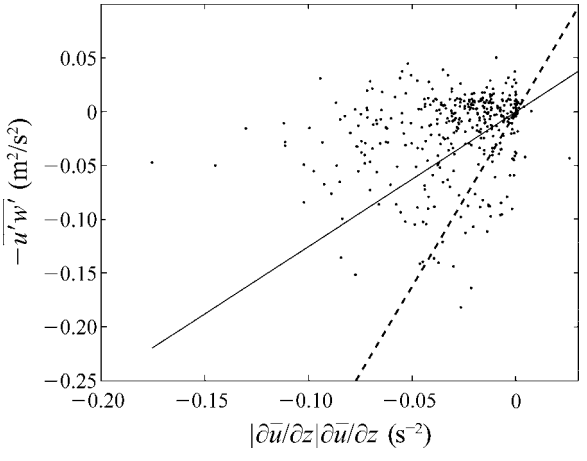

FIG. 12. The variation of measured $-\overline{u'w'}$ at the edge with measured $|\partial\bar{u}/\partial z|\partial\bar{u}/\partial z$ for northerly wind directions. The slope is the square of the effective mixing length (l) for momentum transfer. For reference, the classical boundary layer length scale $l = k_v z$ (solid line; where k_v is the Von Karman constant) and the canopy mixing length $l = 0.1\ h_c$ (dashed line) are shown.

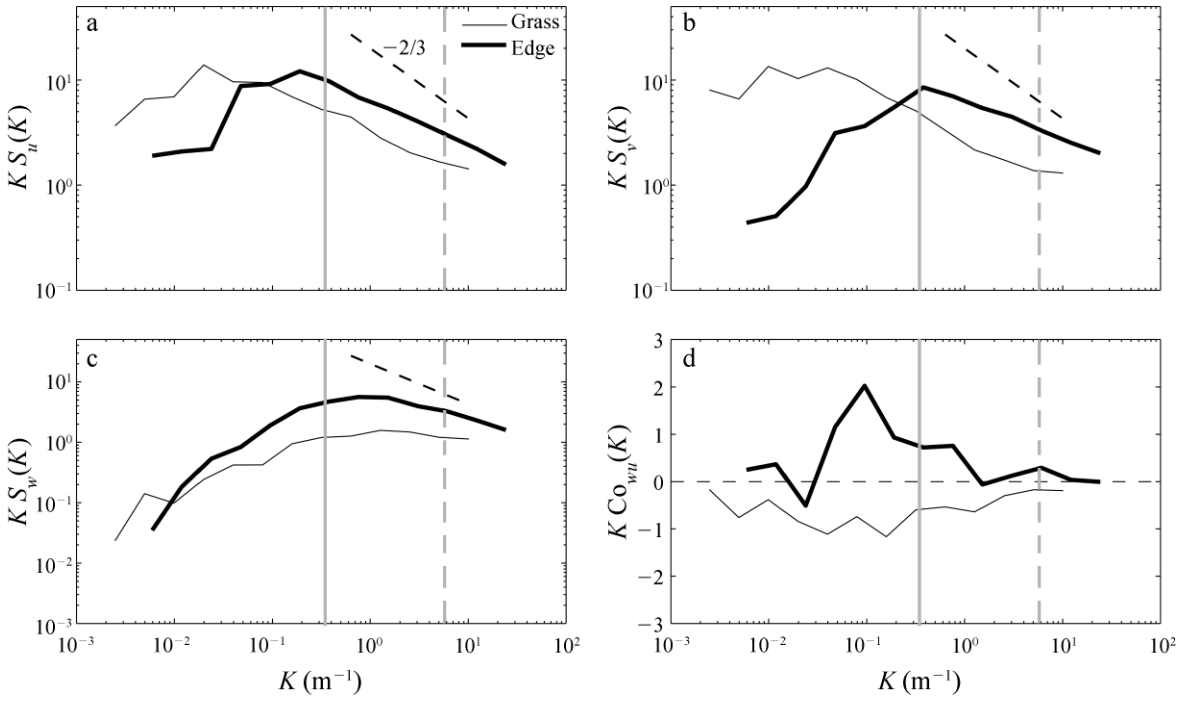

FIG. 13. The Haar wavelet energy spectra (S) at the edge and at the center of the grass clearing for (a) $u'(S_u)$, (b) $v'(S_v)$, and (c) $w'(S_w)$ as a function of wave number ($K = 2\pi/R$), where R is a length scale. (d) Their co-spectral Co_{uw} variations. The two vertical gray lines represent wave numbers corresponding to $R = k_v z$ (dashed line) and $R = h_c$ (solid line). The inertial sub-range slope ($= -2/3$) is shown for reference.

the production mechanism between u' and v' (as alluded to in Eq. 1).

The surprising results were for measured co-spectral (Co_{uw}) dissimilarity between the edge and the central tower within the grass site. For almost all the runs we analyzed (not shown), with mean wind directions from the north (forest-to-clearing), $K\ \mathrm{Co}_{uw}$ was positive between length scales ranging from $2h_c$ to $k_v z/2$ at the edge but consistently negative at the grass tower. At scales larger than $2h_c$, $K\ \mathrm{Co}_{uw}$ at the edge fluctuated in sign among various runs, but remained positive between $2h_c$ and $k_v z/2$. This co-spectral analysis suggests that eddies responsible for the positive $\overline{u'w'}$ (and hence a potential re-circulation in the BFS analogy) are larger than $k_v z$ (the boundary layer mixing length over the grass) but are not much larger than the canopy height, again consistent with the recirculation size in Fig. 1.

Summary and Conclusions

Using an array of three sonic anemometers positioned near a tall pine forest edge, we showed that when the mean wind direction is from the forest into a large grass-covered clearing:

1) The measured $\partial\bar{u}/\partial z < 0$, $\partial\bar{u}/\partial x < 0$, $\bar{w} > 0$ and $\partial\bar{w}/\partial z > 0$, $\partial\bar{w}/\partial x > 0$, $\overline{u'w'} > 0$ and $\partial\overline{u'w'}/\partial z > 0$, $\partial\overline{u'^2}/\partial x < 0$, and $\partial\overline{w'^2}/\partial x < 0$ are all consistent with an intermittent recirculation pattern whose genesis is a backward-facing step (BFS) flow.

2) The mean trend in estimated $-\rho^{-1}\partial\bar{p}/\partial x$ becomes increasingly negative with increasing $\bar{u}^2$ consistent with ground pressure measurements reported in other forest to clearing edge studies.

3) The mixing length scale for momentum transfer at the edge is not well defined but its scatter is bounded by values less than $k_v z$ to values exceeding $0.1h_c$.

4) The measured co-spectra of $\overline{u'w'}$ is positive between the length scales ranging from $2h_c$ to $k_v z$, scales comparable to the expected BFS recirculation size.

Disentangling the signature of the BFS flow regime at various locations in forest clearings from other flow regimes is the next logical step that can benefit from a broader set of experiments, visualizations, and simulations. Intensive field experiments (including smoke visualization already used by Bergen 1975), flume and wind tunnel flow visualization experiments, and large eddy simulations (LES) can all be utilized to further explore the external conditions promoting the onset of the BFS regime at edges and its contribution to various flow statistics.

Another finding from this experiment is the differences in adjustments among the second order statistics as the flow exits the forest canopy. We showed that the lateral velocity variance, $\overline{v'^2}$, is the moment that adjusts most slowly. Surprisingly, the longitudinal and vertical velocity variances ($\overline{u'^2}$ and $\overline{w'^2}$) at the forest edge were comparable to their respective values at the center of the clearing suggesting rapid adjustment at the edge.

Qualitatively, we showed that the only mechanism that can modulate $\overline{v'^2}$ as the flow exits the forest edge is the flux transport term, known to be less efficient. This finding has important implications for two-equation ($k - \varepsilon$) or other Reynolds-averaged Navier-Stokes (RANS) closure models used to compute flows near forest edges because the $\overline{v'^2}$ budget is rarely considered in such models.

Finally, a unique data set was collected for the mean flow and second moment statistics along with their horizontal and vertical gradients near a tall forest edge referenced to the flow statistics that are in quasi-equilibrium with the forest clearing. These data can guide future LES with a lens on developing realistic subgrid closure schemes that account for features that appear sharp in space but are "porous" to current fluid dynamics subgrid models.

Ecological Applications

Fragmented landscapes are becoming widespread features of the modern world resulting in abrupt increases in artificial forest edges (Laurence 2004). Understanding how the creation of such artificial forest edges affect the neighboring physical and biological environment remains a central research topic in applied ecology. Here, we focused on quantifying how dense forest edges alter the structure of the mean and turbulent wind in the immediate vicinity of a tall forest edge. Our experiments show that a re-circulation pattern, whose genesis is analogous to a BFS flow, significantly impacts all the terms in the longitudinal mean momentum equation. This is the first "field evidence" documenting the importance of a BFS-like phenomenon on key terms in the mean longitudinal momentum equation. Such a recirculation zone can lead to disproportionate trapping and re-suspension of seeds and other airborne organisms originating from within the canopy into the canopy gaps.

Acknowledgments

This research was supported by the Office of Science (BER), U.S. Department of Energy, through the Terrestrial Carbon Processes Program (TCP) grant no. DE-FG02-00ER63015 and grant no DEFG02-95ER62083, and through BER's Southeast Regional Center (SERC) of the National Institute for Global Environmental Change (NIGEC) under Cooperative Agreement no. DEFC02-03ER63613, and by the National Science Foundation's Earth Science Division (NSF-EAR 02-08258).

Literature Cited

Armali, F., F. Durst, J. C. F. Pereira, and B. Schonung. 1983. Experimental and theoretical investigation of backward facing step flow. Journal of Fluid Mechanics 127:473–496.

Baldocchi, D. D., et al. 2001. FLUXNET: a new tool to study the temporal and spatial variability of ecosystem-scale carbon dioxide, water vapor and energy flux densities. Bulletin of the American Meteorological Society 82:2415–2435.

Belcher, S. E., N. Jerram, and J. C. R. Hunt. 2003. Adjustment of a turbulent boundary layer to a canopy of roughness elements. Journal of Fluid Mechanics 488:369–398.

Bergen, J. 1975. Air movement in a forest clearing as indicated by smoke drift. Agricultural Meteorology 15:165–179.

Chun, K. B., and H. J. Sung. 1998. Visualization of a locally-forced separated flow over a backward-facing step. Experiments in Fluids 25:133–142.

Coceal, O., and S. E. Belcher. 2005. Mean winds through an inhomogeneous urban canopy. Boundary-Layer Meteorology 115:47–68.

Dejoan, A., and M. A. Leschziner. 2004. Large eddy simulation of periodically perturbed separated flow over a backward-facing step. International Journal of Heat and Fluid Flow 25: 581–559.

De Ridder, K., B. Neirynck, and C. Mensink. 2004. Parameterising forest edge deposition using effective roughness length. Agricultural and Forest Meteorology 123:1–11.

Dwyer, M. J., E. G. Patton, and R. H. Shaw. 1997. Turbulent kinetic energy budgets from a Large-Eddy Simulation of airflow above and within a forest canopy. Boundary-Layer Meteorology 84:23–43.

Flesch, T. K., and J. D. Wilson. 1999. Wind and remnant tree sway in forest cutblocks. I. Measured winds in experimental cutblocks. Agricultural and Forest Meteorology 93:229–242.

Furuichi, N., T. Hachiga, and M. Kumada. 2004. An experimental investigation of a large-scale structure of a two-dimensional backward-facing step by using advanced multi-point LDV. Experiments in Fluids 36:274–281.

Gardiner, B. A. 1994. Wind and wind forces in a plantation spruce forest. Boundary-Layer Meteorology 67:161–186.

Garratt, J. R. 1990. The internal boundary-layer: a review. Boundary-Layer Meteorology 50:171–203.

Garratt, J. R. 1994. The atmospheric boundary-layer: review. Earth-Science Reviews 37(1–2)89–134.

Irvine, M. R., B. A. Gardiner, and M. K. Hill. 1997. The evolution of turbulence across a forest edge. Boundary-Layer Meteorology 84:467–496.

Juang, J. Y., G. G. Katul, M. Siqueira, P. Stoy, S. Palmroth, H. R. McCarthy, H. S. Kim, and R. Oren. 2006. Modeling nighttime ecosystem respiration from measured CO_2 concentration and air temperature profiles using inverse methods. Journal of Geophysical Research 111:D08S05. [doi: 10.1029/2005JD005976]

Judd, M. J., M. R. Raupach, and J. J. Finnigan. 1996. A wind tunnel study of turbulent flow around single and multiple windbreaks. Part I: velocity fields. Boundary-Layer Meteorology 80:127–165.

Kaimal, J. C., and J. J. Finningan. 1994. Atmospheric boundary layer flows. Oxford University Press, Oxford, UK.

Katul, G. G., and J. D. Albertson. 1998. An investigation of higher order closure models for a forested canopy. Boundary-Layer Meteorology 89:47–74.

Katul, G. G., J. D. Albertson, C. I. Hsieh, P. S. Conklin, J. T. Sigmon, M. B. Parlange, and K. R. Knoerr. 1996. The inactive eddy-motion and the large-scale turbulent pressure fluctuations in the dynamic sublayer. Journal of the Atmospheric Sciences 53:2512–2524.

Katul, G. G., and W. H. Chang. 1999. Principal length scales in second-order closure models for canopy turbulence. Journal of Applied Meteorology 38:1631–1643.

Katul, G. G., and C. R. Chu. 1998. A theoretical and experimental investigation of the energy-containing scales in the dynamic sublayer of boundary-layer flows. Boundary-Layer Meteorology 86:279–312.

Katul, G. G., C. I. Hsieh, and J. Sigmon. 1997. Energy-inertial scale interaction for temperature and velocity in the unstable surface layer. Boundary-Layer Meteorology 82:49–80.

Katul, G. G., M. B. Parlange, and C. R. Chu. 1994. Intermittency, local isotropy, and non-Gaussian statistics in atmospheric surface layer turbulence. Physics of Fluids 6: 2480–2492.

Katul, G. G., B. Vidakovic, and J. D. Albertson. 2001. Estimating global and local scaling exponents in turbulent flows using wavelet transformations. Physics of Fluids 13: 241–250.

Klaassen, W. 1992. Average fluxes from heterogeneous vegetated regions. Boundary-Layer Meteorology 58:329–354.
Klaassen, W., and M. Claussen. 1995. Landscape variability and surface flux parameterization in climate models. Agricultural and Forest Meteorology 73:181–188.
Kostas, J., J. Soria, and M. S. Chong. 2002. Particle image velocimetry measurements of a backward-facing step flow. Experiments in Fluids 33:838–853.
Laurence, W. 2004. Forest–climate interactions in fragmented tropical landscapes. Philosophical Transactions of the Royal Society of London 359:345–352.
Lee, X. 2000. Air motion within and above forest vegetation in non-ideal conditions. Forest Ecology and Management 135: 3–18.
Li, Z., J. D. Lin, and D. R. Miller. 1990. Airflow over and through a forest edge: a steady-state numerical-simulation. Boundary Layer Meteorology 51:179–197.
Malcom, J. R. 1998. A model of conductive heat flow in forest edges and fragmented landscapes. Climate Change 39:487–502.
McNaughton, K. G. 1989. Micrometeorology of shelter belts and forest edges. Philosophical Transactions of the Royal Society of London B324:351–368.
Morse, A. P., B. A. Gardiner, and B. J. Marshall. 2002. Mechanisms controlling turbulence development across a forest edge. Boundary-Layer Meteorology 103:227–251.
Nakagawa, H., and I. Nezu. 1987. Experimental investigation on turbulent structure of a backward facing step flow in an open channel. Journal of Hydraulic Research 25:67–88.
Nathan, R., and G. G. Katul. 2005. Foliage shedding in deciduous forests lifts up long-distance seed dispersal by wind. Proceedings of the National Academy of Sciences (USA) 102:8251–8256.
Nathan, R., G. G. Katul, H. S. Horn, S. M. Thomas, R. Oren, R. Avissar, S. W. Pacala, and S. A. Levin. 2002. Mechanisms of long-distance dispersal of seeds by wind. Nature 418:409–413.
Nathan, R. N., N. Sapir, A. Tracktenbrot, G. G. Katul, G. Bohrer, M. Otte, R. Avissar, M. B. Soons, H. S. Horn, M. Wikelski, and S. Levine. 2005. Long-distance biological transport processes through the air: Can nature's complexity be unfolded in silicon? Diversity and Distributions 1:131–137.
Nezu, I. 2005. Open-channel flow turbulence and its research prospect in the 21st century. Journal of Hydraulic Engineering 131:229–246.
Nieveen, J. P., R. M. M. El-Kilani, and A. F. G. Jacobs. 2001. Behaviour of the static pressure around a tussock grassland-forest interface. Agricultural and Forest Meteorology 106: 253–259.
Novick, K. A., P. C. Stoy, G. G. Katul, D. S. Ellsworth, M. B. S. Siqueira, J. Juang, and R. Oren. 2004. Carbon dioxide and water vapor exchange in a warm temperate grassland. Oecologia 138:259–274.
Patton, E. G., R. H. Shaw, M. J. Judd, and M. R. Raupach. 1998. Large-eddy simulation of windbreak flow. Boundary-Layer Meteorology 87:275–306.
Piirto, M., P. Saarenrinne, H. Eloranta, and R. Karvinen. 2003. Measuring turbulence energy with PIV in a backward-facing step flow. Experiments in Fluids 35:219–236.
Poggi, D., G. G. Katul, and J. D. Albertson. 2004. Momentum transfer and turbulent kinetic energy budgets within a dense model canopy. Boundary-Layer Meteorology 111:589–614.
Rao, K. S, J. C. Wyngaard, and O. R. Coté. 1974. The structure of the two-dimensional internal boundary layer over a sudden change of surface roughness. Journal of the Atmospheric Science 31:738–746.
Raupach, M. R., E. F. Bradley, and H. Ghadiri. 1987. Wind tunnel investigation into the aerodynamic effect of forest clearing of the nesting of Abbott's Booby on Christmas Island. Progress Report, CSIRO Division of Environmental Mechanics, Canberra, Australia.
Raupach, M. R., and R. H. Shaw. 1982. Averaging procedures for flow within vegetation canopies. Boundary-Layer Meteorology 22:79–90.
Raynor, G. S. 1971. Wind and temperature structure in a coniferous forest and a contiguous field. Forest Science 17: 351–363.
Scarano, F., C. Benocci, and M. L. Riethmuller. 1999. Pattern recognition analysis of the turbulent flow past a backward facing step. Physics of Fluids 11:3808–3818.
Schram, C., P. Rambaud, and M. L. Riethmuller. 2004. Wavelet based eddy structure deduction from a backward facing step flow investigated using particle image velocimetry. Experiments in Fluids 36:233–245.
Shaw, R. H. 1977. Secondary wind speed maxima inside plant canopies. Journal of Applied Meteorology 16:514–521.
Sheu, T. W. H., and H. P. Rani. 2006. Exploration of vortex dynamics for transitional flows in a three-dimensional backward-facing step channel. Journal of Fluid Mechanics 550:61–83.
Simpson, R. 1989. Turbulent boundary layer separation. Annual Reviews of Fluid Mechanics 21:205–234.
Siqueira, M., and G. G. Katul. 2002. Estimating heat sources and fluxes in thermally stratified canopy flows using higher-order closure models. Boundary-Layer Meteorology 103: 125–142.
Soons, M. B., G. W. Heil, R. Nathan, and G. G. Katul. 2004. Determinants of long distance dispersal by wind in grasslands. Ecology 85:3056–3068.
Spazzini, P. G., G. Iuso, M. Onorato, N. Zurlo, and G. M. D. Cicca. 2001. Unsteady behaviour of backfacing step flow. Experiments in Fluids 30:551–561.
Stoy, P., G. G. Katul, M. Siqueira, J. Y. Juang, H. R. McCarthy, H. S. Kim, A. C. Oishi, and R. Oren. 2005. Variability in net ecosystem exchange from hourly to inter-annual time scales at adjacent pine and hardwood forests: a wavelet analysis. Tree Physiology 25:887–902.
Veen, W. L., W. Klaassen, B. Kruijt, and R. W. A. Hutjes. 1996. Forest edges and the soil–vegetation–atmosphere interaction at the landscape scale: the state of affairs. Progress in Physical Geography 20:292–310.
Williams, C., S. Ladeau, R. Oren, and G. G. Katul. 2006. Modeling seed dispersal distances: implications for transgenic *Pinus taeda*. Ecological Applications 16:117–124.
Wilson, N. R., and R. H. Shaw. 1977. A higher order closure model for canopy flows. Journal of Applied Meteorology 16: 1198–1205.